5. Aharonov-Bohm effect and persistent currents in non-superconducting systems

Keywords: phase coherence; fluxquantum; diffusive transport; thermodynamic equilibrium; energy eigenstates;

5.1 Introduction

In the classical Drude description of transport of electrons in the solid state (see chapter 2, section 2) it is assumed that, whenever an electron scatters, all information on its previous state will be lost. As we have seen in chapter 1 such loss of information only occurs in the case of inelastic scattering events, where each particular scattering event is unpredictable in both time and position. In contrast, elastic scattering affects the trajectory of the travelling electron in such a way that the phase shift resulting after the scattering event can be predicted. Consequently this will lead to quantum interference of the electronic wavefunction over a length scale determined by inelastic processes, a size which commonly is much larger than the elastic mean free path (e.g., see chapter 2, section 3). In addition, this not only holds for a single electron, but also for the average effect of a number of electrons, i.e. it affects the conductance.
In this chapter we will discuss two particular effects which clearly demonstrate this quantum interference, both occurring in small ring-shaped structures. These are the Aharonov-Bohm effect and the phenomenon of persistent currents in normal (i.e. non-superconducting) conductors. The two effects are discussed here sequentially as they are connected rather strongly.

5.2 Aharonov Bohm effect in the solid state

In this section we introduce the effect of a magnetic field on the electron transport through ring-shaped conductors at low temperatures, such that phase coherence of the electron wavefunction in the ring is (at least partially) preserved. We will see that the flux enclosed by the ring modulates the total transmission through the ring with a period of either one flux quantum or half of it. This periodic flux dependent modulation leads to an oscillatory behaviour of the conductance versus the applied B-field. The amplitude of this oscillatory part is found to be $\sim 2e^2/h$ at low temperature and low voltage across the ring terminals. Increasing these leads to suppression of this amplitude, and we will see that the characteristic energy scale is given by the Thouless energy, introduced in chapter 1. We will also see how averaging over an ensemble of (nominally equal) rings will lead to suppression of the one-flux quantum periodicity while preserving the half-flux quantum contribution. After a brief introduction to the effect, we continue with a theoretical discussion of the subject in subsection 5.2.a., followed by a few important experimental results (subsection 5.2.b.).

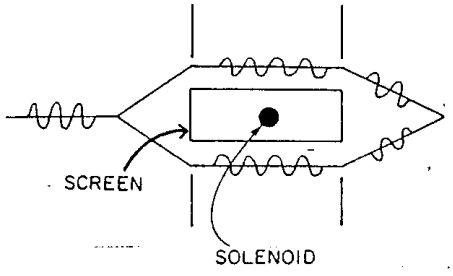

Fig. 5.1. Aharonov-Bohm configuration. The solenoid generates a magnetic field, with the shield preventing the field to be present at the trajectories of the electron.

The Aharonov-Bohm (AB) effect bears its name after Aharonov and Bohm who presented a thought experiment, describing how a magnetic flux affects the interference of a split electron wave [Phys Rev. 115, 485 (1959)]. The most essential aspect of the "experiment" is that it unambiguously confirms the physical reality of the *magnetic vector potential*, raising it from a mathematical entity to a true physical quantity. Fig. 5.1 shows the basic features of the experiment. An electron wave emitted from a source is split into two partial waves which are recombined at a further distance, effectively forming an electron interferometer. The two partial waves enclose a flux localised in the area between the two waves, such that *no magnetic field exists anywhere along the path of the electron waves*. However, despite the absence of a magnetic field all the way along the trajectories (and so *without* the Lorentzforce acting on the particle!), the *vector potential* associated with the field can not taken to be zero everywhere along a closed path, irrespective what gauge is chosen.
Quantum mechanically we know that the vectorpotential A modifies the canonical momentum of an electron with charge $-e$ travelling at a velocity v according to

$$p = hk/2\pi = mv + eA \qquad (5.1)$$

A change in momentum implies a change in phase acquired by the electron after travelling a certain distance (see also below). So, a magnetic field which may be zero at the actual electron trajectory, still affects the phase of the electron wave via the vector potential.
It took quite some time before this rather remarkable fact became accepted, and even now the discussion is not fully completed, despite the indisputable experimental confirmation of the effect for electrons in free space (A. Tonomura et.al., Phys Rev. Lett. 48, 1443 (1982); A. Tonomura et.al., Phys. Rev. Lett. 56, 792 (1986)). Although of considerable fundamental interest, we will not discuss these experiments in detail but continue with the theory for electrons in a solid.

The total phase acquired by a propagating electron along some path described by a position variable l immediately follows from the canonical momentum of eq. (5.1)

$$\Delta\phi = \int \vec{k}.d\vec{l} = \frac{1}{\hbar}\int (m\vec{v} + e\vec{A})d\vec{l} = \Delta\phi_v + \Delta\phi_A \qquad (5.2)$$

i.e. the sum of a contribution due to the velocity v of the particle and one resulting from the vectorpotential A. Thus, the phase shift induced by the vectorpotential is given by

$$\Delta\phi_A = \frac{e}{\hbar}\int \vec{A}.d\vec{l} \qquad (5.3a)$$

and so the phase shift induced by the vectorpotential on an electron propagating once around a closed loop is found as

$$\Delta\phi_A = \frac{e}{\hbar}\oint \vec{A}.d\vec{l} = \frac{e}{\hbar}\iint (rot\vec{A}.d\vec{S} = \frac{e}{\hbar}BS = 2\pi\frac{\Phi}{\Phi_0} \qquad (5.3b)$$

with Φ_0 being the flux quantum h/e. So the phase difference equals 2π *times the enclosed flux in units of the flux quantum* Φ_0. As a phase difference is only distinguishable Mod(2π) *any* effect resulting from this enclosed flux will show a periodic behaviour, with a period of one flux quantum. The enclosed flux is often referred to as the *Aharonov-Bohm-* or *AB-flux.*

5.2.a. *The Aharonov-Bohm and Altshuler-Aronov-Spivak effects in the solid state*

We want to investigate how the Aharonov-Bohm effect manifests itself in the solid state. We concentrate on electrons in metallic structures in the quantum diffusive regime, i.e. $l_e << l_\phi \sim < L$, with L denoting the size of the AB structure, more specifically the length of the circumference of the ring. Contrary to the original AB experiment, in these structures the magnetic field commonly is not confined to the centre of the ring or loop only, but it will also penetrate the metal where the electrons reside, i.e. the electrons experience the B-field in this case. Despite this (rather fundamental!) difference, also in the solid state the effect is called the Aharonov-Bohm effect.
Figure 5.2 shows a ring of small crossection, with two diametrically positioned leads attached at the junctions J_1 and J_2 to allow conductance measurements. An external magnetic field induces a flux Φ in the ring. Two types of trajectories are shown, one connecting the input junction (J_1) to the output (J_2), and the second type returning the particle to the input junction. In figure 5.2a two paths 1 and 2 of lengths L_1 and L_2 respectively ($L_1 \sim L_2$) run along the "top" and "bottom" branch of the ring, each path covering only half of the circumference L of the ring. In b. the paths 3 and 4 fully encircle the loop clockwise and counter clockwise respectively.
Let us first concentrate on the trajectories of the type 1 and 2 shown in figure 5.2a. The acquired difference in AB phase between the two paths follows directly from eq. (5.3b), with half of the total AB phase lagging (i.e. with negative sign) along one path and the other half leading (positive sign) along the second path. Consequently the phase difference will increase

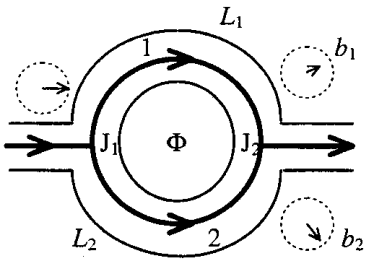

a.

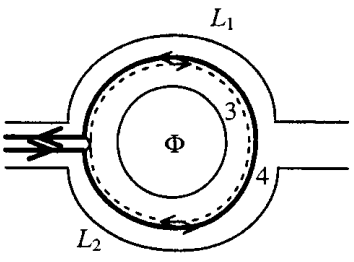

b.

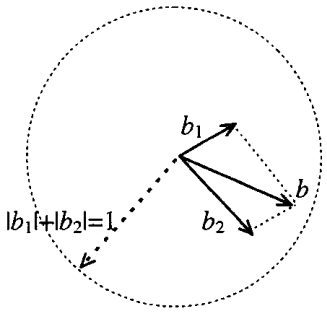

c.

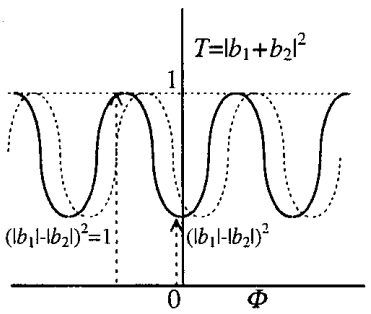

d.

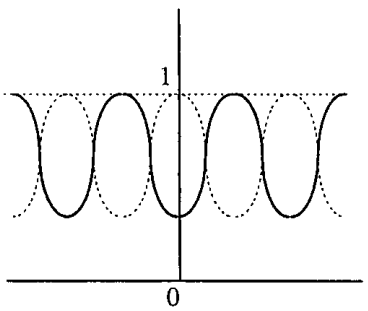

e.

Figure 5.2. Simplified picture of the electron wave interference in a conducting ring. Two types of trajectories contributing to the AB effect are shown. J_1 is (arbitrarily) taken as the junction with the input lead and J_2 that for the output side; a.: two semicircular orbits 1 & 2 leading to coherent forward scattering; b.: two full circular orbits 3 (dashed line) & 4 (solid line) leading to coherent backscattering; c. vectorial summation of output wave amplitudes; d. total transmission probability $T=|b_1+b_2|^2$ (solid line is for identical path lengths 1 & 2; dashed line for non-identical path lengths). A more elaborate evaluation shows that the oscillation at $\Phi=0$ can not take any random value between the extrema, but is either maximum or minimum, i.e. the phase is either $\Delta\phi=0$ or $\Delta\phi=\pi$. This is shown in e.

by 2π each time one flux quantum is added to the ring. So the period of the AB oscillations resulting from these types of trajectories equals Φ_0 or h/e.

In chapter 2 we have seen that, based on the Landauer approach, the conductance of a system is determined by the transmission probability of the electron waves. So, to calculate the conductance of the ring we have to evaluate the total transmission probability for a unity incoming wave from (e.g.) the left lead, splitting at the entrance junction J_1, each partial wave travelling along its respective path and recombining at J_2, *taking into account the phase acquired by each partial wave.* We first will give a simplified picture of the resulting interference of the electron waves, and discuss and correct one error that results from this simplified picture afterwards.
Let us write a_1 and a_2 for the amplitudes of the partial waves in path 1 and 2 leaving the wave-splitter J_1, and b_1 and b_2 for the waves arriving at J_2 to form the output wave (fig. 5.2a). With unity incoming wave, $|a_1+a_2|^2=1$ the total transmission probability T is derived from the *vector summation* of the partial waves b_1 and b_2, yielding $T=|b_1+b_2|^2$ (figure 5.2c and d). We simply can write

$$b_j = a_j F(L_j)\exp(-i\Delta\phi_j) = a_j F(L_j)\exp(-i(\Delta\phi_{v,j} + \Delta\phi_{A,j})) \qquad (j=1,2) \qquad (5.4)$$

with $\Delta\phi_{v,j}$ denoting the acquired phase at zero B field for the partial wave along path j, etc. The prefactor $F(L_j)$ is real and we assume it to be 1 for the moment.
For the transmission probability T we thus find

$$T = a_1^2 F^2(L_1) + a_2^2 F^2(L_2) + 2a_1 a_2 F(L_1)F(L_2)\cos(\Delta\phi_1 - \Delta\phi_2) \qquad (5.5)$$

In an ideal, perfectly symmetric ring both the lengths of the trajectories 1 and 2 as well as the amplitudes of the partial wave amplitudes a_j for the two paths ($a_1 = a_2 = \frac{1}{2}\sqrt{2}$) are equal. The equality of the length implies that also the phase differences $\Delta\phi_{v,j}$ for the two paths will be the same. At zero magnetic field the two partial waves will arrive at the output terminal with the same phase, i.e. $\cos(\Delta\phi_1 - \Delta\phi_2)=1$. From eq. (5.5) we see that this constructive interference yields a *maximum* total (forward) transmission probability T of the wavefunction at the output lead, or *a maximum of the conductance* through the ring (fig. 5.2d, solid curve). With the assumption $F(l)=1$ we find $T=1$, i.e. unity conductance at $B=0$ or $\Phi=0$. At non-zero flux a non-zero phase difference will result from the vector potential term and so the cosine term in eq. (5.5) will become <1 (fig. 5.2c). In particular at $\Phi=\Phi_0/2$ the cosine will be -1, leading to a full suppression of the transmission, i.e. zero conductance or infinite resistance of the loop. Thus, the resistance is found to oscillate with the applied flux, with a period given by a flux quantum penetrating the ring. The size of the oscillation is governed by the ratio of the two output partial waves b_1 and b_2.
To fulfil the conditions for a ring to be ideal we have to realise that the zero flux phase difference result from the difference in path length of the two halves of the ring, taken in units of the Fermi wavelength λ_F. In a metal λ_F equals a few tenths of a nm. This would imply that the fabrication of these rings should be accurate to better than 0.1 nm, a condition which can not be met using present day technology (see Appendix A). So, in a realistic ring the two halves of the loop will not be identical and thus the phase difference on arrival at the output at zero B-field will not be zero. As the phases will depend on the *specific microscopic details of the two trajectories*, its difference $\Delta\phi(\Phi=0)$ at arrival will have a *random value* anywhere between $-\pi$ and $+\pi$, making the total transmission to lay

somewhere in between the maximum and minimum *at random at* Φ=0 (fig. 5.2d, dashed curve).
The picture we presented above provides a transparent view of the way electron wave interference leads to AB oscillations. However, as we mentioned at the beginning, it is highly simplified. If a more elaborate approach is taken the main modification that follows relates to the zero-flux phase of the oscillation. In the preceding discussion we "forgot" to take into account that, at (e.g.) the exit splitter a certain fraction of the wave that approaches the splitter via one arm does not leave the ring but "crosses over" and continues into the other arm, somewhat similar to the AAS type of contribution. This has consequences for the zero-flux phase. While the simple picture yields a random value for it, i.e. $-\pi<\Delta\phi(\Phi=0)<-\pi$, the more complete calculation shows that $\Delta\phi(\Phi=0)$ is *either* 0 *or* π. Now it is found that the randomness associated with the microscopic details of the ring enters in a different way, namely *which* of the two values is assumed in a particular case is again *random*. This is shown in figure 5.2e by the solid and dashed curves. As just briefly mentioned, it is the accounting for the wave that continues inside the ring after a splitter that is the key element for this *symmetry* of the transmission (and conductance) around zero flux. Basically this "accounting" guarantees that we meet the fundamental requirement of conservation of particles in the transmission process through the structure, with in addition the condition for time-reversal symmetry at zero magnetic field. Note that the first of the two conditions is quantummechanically equivalent to the conservation of wavefunction probability $|\Psi|^2$. One step further, the correct way of keeping track of the wavefunction probability implies that we allow the formation of *well-defined eigenstates* in the ring. We will return to this aspect in section 5.3 on persistent currents in normal (= non-superconducting) conductors, where the existence of these eigenstates is at the key element for the occurrence of such currents.

In a realistic ring two more influences have to be accounted for. Just as the lengths of the two halves may differ, also the junctions may show asymmetries in their wave splitting (and combining) properties. This implies that the amplitudes a_j will differ. From eq. (5.5) it can be seen immediately that T_{max} will be kept equal to 1. However, the minimum transmission will become finite, i.e. $T_{min}>0$. This implies a *reduction* of the amplitude of the AB resistance (or conductance) oscillation (see figure 5.2d).

In our preceding discussion we assumed that the *total* incoming wave intensity arrives at the output junction, i.e. in eq. (5.4) we took the prefactors $F(L)$=1. This will no longer hold when *scattering* is taken into account: any scattering of the electron(-wave) while traversing the arms, either elastic or inelastic, will reduce the transmitted amplitude, making $F(L_j)<1$. However, the way the two different scattering mechanisms affect the transmitted amplitudes differs considerably.
Inelastic scatterings will reduce the phase coherence during the travelling of the waves along the respective paths. So, the resulting *phase coherent amplitude*, which is the *only relevant contribution* to the AB effect, will be governed by an exponential decay in dependence of the path length l in terms of the phase coherence length l_ϕ, i.e. given by $\exp(-L_j/l_\phi)$. This loss of phase coherence thus is accounted for by multiplying the total transmission T of eq. (5.5) by a factor

$$G(l_\phi)=exp(-L_1/l_\phi).exp(-L_2/l_\phi)=exp(-L/l_\phi) \qquad (5.6)$$

with L denoting the length of the circumference of the ring. From this it is clear that the phase coherence length is the relevant length scale governing the maximum size a loop may have to display these phenomena, i.e. preferably the diameter should be not too large compared to l_ϕ.
The effect of *elastic* scattering on the amplitude is not so simple to evaluate quantitatively. Initially an elastic scatterer will reduce the amplitude of the forward travelling wave in an arm. However, the wave thus reflected may become re-reflected by a scatterer lying more "upstream" along the path. This process results in multiple elastic scattering leading to a complicated standing wave pattern, the details of which will depend on the *microscopic spatial arrangement* of the individual elastic scatterers. Evidently this process affects both the (zero B-field) phase and amplitude of the wave that ultimately arrives at the output junction, however its complexity prevents a quantitative evaluation. We will return to the problem of the amplitude of AB oscillations after discussing the related AAS oscillations and see that it relates to the problem discussed at the very end of chapter 2, when we very briefly hinted upon Universal Conductance Fluctuations (UCFs).
Despite the complexity introduced by elastic scatterings this has *no effect* on the phase*shift* induced by the magnetic field. This rather remarkable (and counterintuitive) fact is an immediate consequence of the way the vector potential acts along a path, as expressed by eq. (5.3b). From it we read that the field-induced phase shift only relies on the enclosed area S of a closed orbit. So, irrespective of the details of the trajectory (e.g. whether parts of it are traversed more than once due to multiple reflection), at a given field value the acquired phase of eq. (5.3b) will depend only on the fixed area enclosed by the circumference of the ring.

Let us now turn to the second type of trajectories, indicated by 3 and 4 in Fig 5.2b. In contrast to the preceding case these waves encircle the *full* loop, returning to their point of entrance to interfere. This leads to *coherent back scattering* (or reflection), in contrast to the preceding semi-circular trajectories showing coherent forward scattering or transmission (note that both affect the total transmission, as the sum of the probabilities for reflection and transmission equals 1). Apart from this, a more intricate difference between the two types arise.
Assuming only *elastic* scattering processes in the two arms, *any* (clockwise) path 3 can also be traversed in the reverse (counter clockwise) direction, i.e. being a path of the type 4. So, each path 4 can be seen as the *time reversed* trajectory of a path 3, making the phases acquired (at zero flux) for the two partial waves *exactly equal*. This implies that at zero flux the resulting interference will *always* yield the *maximum* total wave amplitude, or maximum *backscattering* probability R. With T=1-R this yields a minimum in the transmission probability from entrance to exit lead and so a maximum in the resistance (minimum in the conductance) of the loop.
At a non-zero flux Φ the complete encircling of the loop (in mutually opposite directions!) leads to the following phase shifts for the waves 3 and 4:

$$\Delta\phi_3 = +2\pi\frac{\Phi}{\Phi_0} \qquad (5.7a)$$

and

$$\Delta\phi_4 = -2\pi\frac{\Phi}{\Phi_0} = -\Delta\phi_3 \qquad (5.7b)$$

implying a total phase difference $\Delta\phi_3$-$\Delta\phi_4$ that is *twice as large* as in the preceding case of the semi-circle trajectories 1 and 2. So, in this case one oscillation period is obtained if the flux through the loop is increased by $\Phi_0/2$, i.e. twice as *small* as before. This is called the $\Phi_0/2=h/2e$, Altshuler-Aronov-Spivak or AAS oscillation, after the persons who were the first to investigate these.

Concerning the effect of scattering all the arguments given before for the common AB effect also apply to the present AAS case.

Problem: The effect of the phase coherence length is to reduce the AB resistance oscillation amplitude. Discuss which will be affected most: the *h/e* or the *h/2e* oscillations.

We now want to return to the problem of how to evaluate the amplitude of AB (and AAS) oscillations. In addition it is highly instructive to discuss how this depends on external parameters such as temperature and applied current or voltage (see also Appendix B). In the preceding discussion we have evaluated the conductance based on the transmission probability of *a single* electron wave (see e.g. eq. (5.6)). We thus did assume that the structure was 1D. This implies that the width of the ring should be on the order of half a Fermi wavelength, i.e. ~0.1 nm in a metal and ~10-20 nm in a 2DEG semiconductor. In real experiments the minimum width of the ring is dictated by fabrication capabilities, so ~30 nm (see Appendix A). So from this experimental constraint it is evident that the single-channel 1D description can be seen as approximate only. The effect of the finite phase coherence length is not modified. In addition also the basic periodicity of one flux quantum is not affected, and it even can be shown that this property is very fundamental holding for a broad variety of conducting systems.
Within the 1D description it is evident that the amplitude of the conductance oscillation (or fluctuation) will always be $< \sim e^2/h$. In the multi-channel case the amplitudes will be affected, in particular via elastic effects. It is of considerable interest that also in this case the amplitude of the conductance fluctuation *again is* $\sim e^2/h$. This behaviour is found to be universal for the quantum diffusive regime, and we discussed it already very briefly at the end of chapter 2. Effectively it seems as if the transmission of the individual channels contributing to the total transmission do not behave independently, but are somehow coupled by a so-called sum rule. This is a very fundamental property of *random quantum systems.*
The next aspect that needs consideration is how the amplitude of the oscillations is affected by external parameters; in particular we will discuss the role of different energy scales in the system, namely the temperature and the applied (measuring) voltage. This will allow us to become acquainted with the role of the Thouless energy in mesoscopic systems (see chapter 1, section 2b).

To see this, we have to evaluate how the interference of an electron depends on its energy. The kinetic energy of the electrons affects their phases via the velocity or the ν-vector acting in the first term of eq. (5.2). From the eqs. (1.17) and (1.18) in chapter 1 it is seen that the *typical* change of energy ΔE that yields a change in phase of π, -which by definition is the Thouless energy E_{Th}-, is given by $\Delta E=E_{Th}=(h/2\pi)/\tau_L$, with τ_L being the time it takes for an electron to travel the (characteristic) size of the system L. So let us compare the interference of electrons at two energies, E and $E'=E+E_{Th}$. If we assume that the electron at energy E leads to *constructive interference* at the output (i.e. $\Delta\phi_1-\Delta\phi_2=0$ in the last term of eq. (5.5)), then for the electron at the energy E' the additional phase shift of π implies that the term $\Delta\phi_1-\Delta\phi_2=\pi$, or this electron wave experiences *destructive interference*. Thus, we find that the transmission probability T through the ring is energy dependent, including its zero-flux phase. This has a drastic effect on the conductance of the ring. The total conductance of the ring follows from the integration over all contributing electrons (and so over the entire relevant energy range ΔE), divided by that range, or $\frac{1}{\Delta E}\int_{\Delta E} T(E)dE$. If the energy range $\Delta E<<E_{Th}$, the transmission $T(E)$ does not depend on energy and consequently this will hold also for the conductance. If however the system is "fed" by electrons that cover a range $\Delta E>E_{Th}$, we find that part of the electrons interferes constructively while an other part does so destructively, thus reducing the overall (flux dependent oscillatory part of the) conductance. Effectively we may divide the relevant energy interval ΔE into $N_b=\Delta E/E_{Th}$ energy "slices" which have a different amplitude with alternating zero-flux phases. This leads to partial cancellation. So in conclusion, *once the energy window of the electrons entering the ring system surpasses the Thouless energy, the amplitude of the oscillatory part of the resistance becomes reduced.* A quantitative analyses shows that the reduction follows $\sqrt{E_{Th}/\Delta E}$. The energy interval ΔE can be controlled by the bias voltage applied across the entrance-exit leads, i.e. $\Delta E=eV_{bias}$, or by the temperature of the electron reservoirs of the leads ($\Delta E\sim 3kT$), and so we envision a bias voltage and a temperature dependence of the AB oscillation amplitudes.

5.2.b. *Experimental results of AB and AAS oscillations.*

Now we are ready to discuss a few experiments on the AB and AAS effect. Figure 5.3 shows a typical sample comprising a small, narrow Au ring fabricated by standard electron-beam lithography and metal evaporation (R.A. Webb et.al, Phys. Rev. Lett. 54, 2696 (1985)). The typical dimensions are 820 nm diameter, 50 nm wirewidth and 40 nm thickness of the Au film. Figure 5.4 shows the results obtained from the measurement of the conductance in dependence of an externally applied magnetic field, at a temperature of 40 mK. The clear, oscillating pattern nicely demonstrates the AB effect in the solid state in the diffusive transport regime to be real. The Fourier transform of the conductance oscillations given in Fig. 5.4b shows a clear peak in "frequency" $1/B$. Taking the surface area enclosed by the loop, this fully complies with the h/e AB oscillation period, i.e. a change of one flux quantum through the loop per oscillation period. Also a

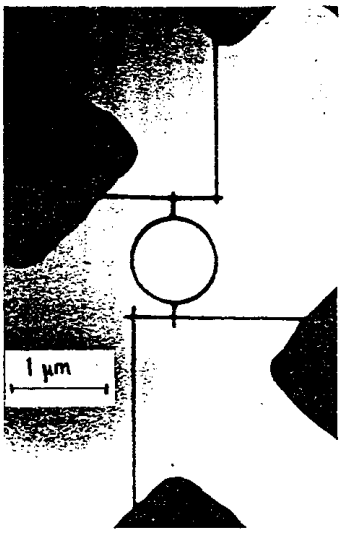

Figure 5.3. A gold ring with four leads (two at the top and left, two at the bottom and right) to study Aharonov-Bohm effects in the quantum diffusive regime.

very weak *h/2e* feature is seen. From more detailed experiments (at large magnetic fields) it became clear that this is a harmonic of the AB oscillation and not an AAS contribution, i.e. not due to time-reversed trajectories. From the discussion on the AB and AAS

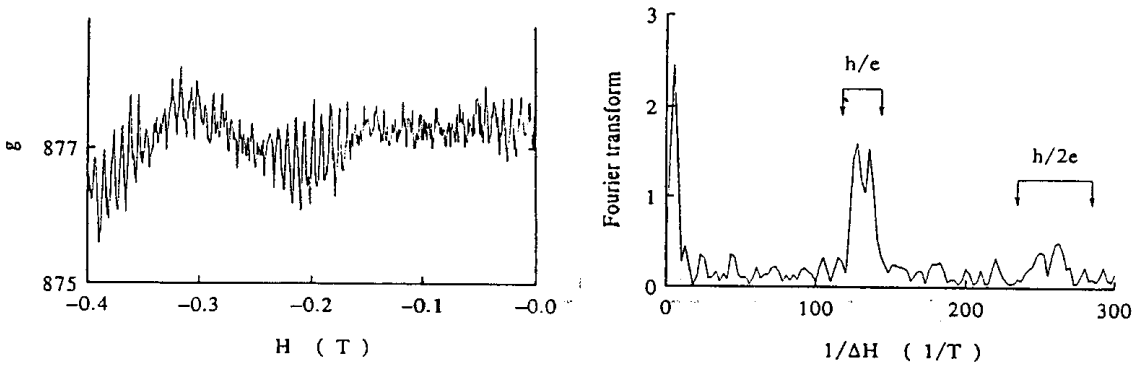

a. *b.*

Figure 5.4. Conductance oscillations in the ring of fig. 5.3, clearly demonstrating the AB effect. a: A sample of the data; b: The Fourier transform of the data of a.

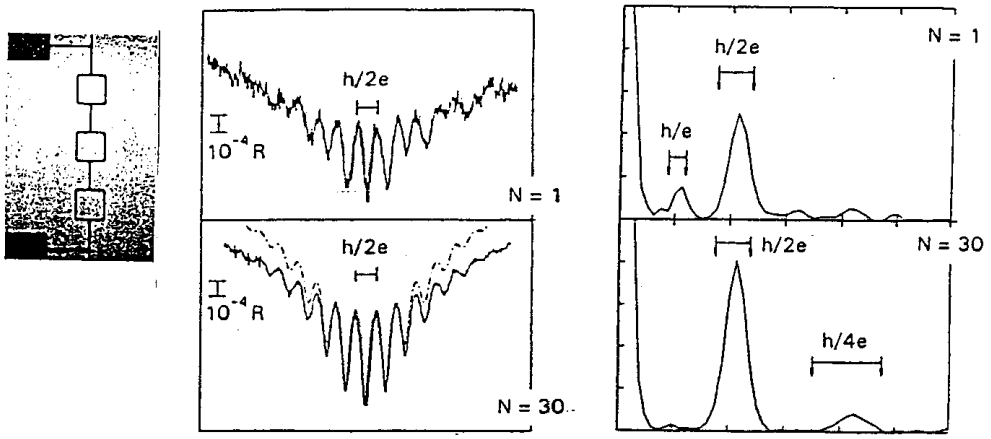

a. *b.* *c.*

Fig 5.5: Ensemble averaging in multi-ring devices. a.: example of a 3-loop structure; b.: resistance data for a single ring (N=1) and the device of N=30 rings; c. Fourier transforms of the data shown in b.

oscillations it became obvious that the first have a phase with a *random value* 0 *or* π of the oscillation at *zero flux*. In contrast, the AAS oscillations, resulting from time reversed path, always will be at a *maximum* resistance at zero flux. This has an immediate consequence on the transport through an ensemble of interconnected rings. For the AB oscillations the total resistance will be a sum of the randomly phased AB contributions and so this will lead to a significant suppression of these *h/e* oscillations. This does not hold for the AAS oscillations. Here the zero flux phase is well determined and so the contributions of all individual rings are added "in phase". This is exactly what is found experimentally.
Figure 5.5 provides data obtained from a series of N=30 loops connected in a (1D) array, compared to a single loop (N=1). Just as an illustration figure 5.5a shows a three-loop device; the 30-loop structure is made in a comparable way. The measured resistance versus the applied field clearly shows an oscillatory shape (Fig. 5.5b). Note that in this case the AAS contribution is larger than the AB part (fig. 5.5b & c), the reason of which we will not discuss here. However, the *h/e* contribution is visible in the single ring while it is fully suppressed in the N=30 ensemble, in accordance with our preceding discussion.

Before closing this section we want to discuss one more experiment, stressing the role of the phase coherence length in these type of experiments. Figure 5.6a shows a peculiar "AB"-configuration, i.e. a long, hollow conducting tube, with the magnetic field directed

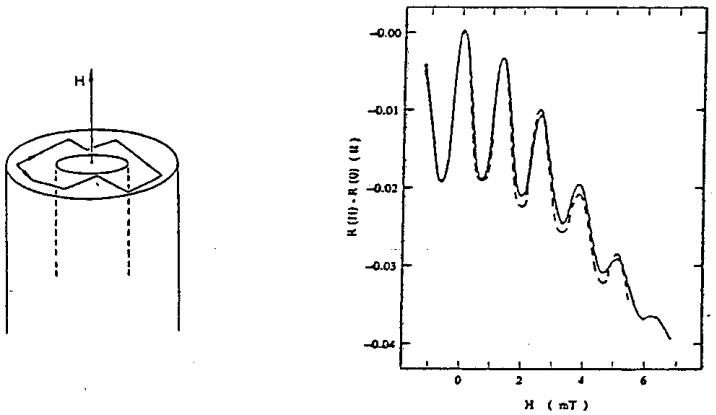

a. b.

Figure 5.6. AAS oscillations in a metal-coated thin glass fibre. a.: The sample configuration; b: Resistance oscillations in dependence of the applied field along the tube.

along the fibre. The tube is made by evaporating a thin metallic layer onto the surface of a glass fibre of typically 1 mm diameter. The length L of ~1mm largely exceeds the phase coherence length l_ϕ. This effectively means that we can subdivide the tube *along its length in ~L/l_ϕ phase independent rings*, each "slice" forming one member of the ensemble of ~L/l_ϕ (>>1) individuals. Because of this large number we anticipate that strong AAS oscillations should be present. This is confirmed in the experiment (figure 5.6b), which shows the results of a measurement of the conductance along the fibre.

5.3 Persistent currents in non superconducting systems

In this section we discuss the phenomenon that a steady state current can exist in a ring shaped conductor. From classical electrodynamics it is known that a current can be set up if a (steady) voltage source or a (time dependent) magnetic field is to generate a current in a closed conductor. Instead, in a mesoscopic structure of ring shaped topology a DC current can arise with a constant, time independent magnetic field. Thus, *the current is a thermodynamic equilibrium property* of the system. It arises if the phase of the electron travelling around the ring is preserved after a full revolution, which gives rise to well defined eigenstates. These states, which are the quantumstates of the electronic system of the whole ring, result in a finite circulating current. The value and direction (or sign) of this current depend on the shape of the energy spectrum and on the occupation of the states of the spectrum. In this way it will be affected by the number of electrons residing in the ring and the magnetic flux enclosed by the ring.

Persistent currents are considerably more familiar then it may seem at first sight. Electrons orbiting the nucleus/i of an atom or a molecule in steady state are well known and understood. These stable electron orbits or states are purely quantum mechanical in origin. Effectively these orbiting electrons form persistent currents and lead to a finite magnetic susceptibility, which can be either dia- or paramagnetic, partially depending on the number of orbiting electrons. Some of these aspects will be discussed in more detail in Chapter 11.
A second example of persistent currents was introduced implicitly in chapter 4. In a 2DEG subject to a large magnetic field the electrons will enter the Integer Quantum Hall state. Under this condition edge states will be formed at the crossing of the Landau levels

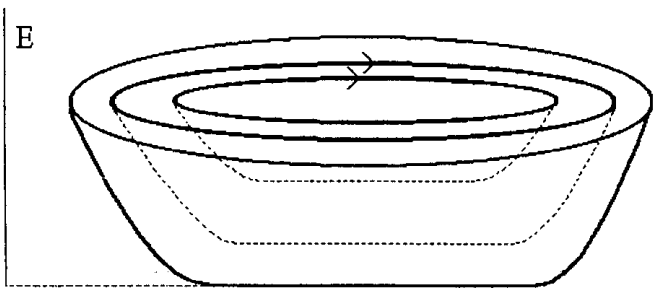

Figure 5.7. Persistent currents in the quantum Hall regime, associated with electrons travelling in edge states along the perimeter of the sample.

and the Fermi energy. Electrons residing in these edge states will travel along the edge of the 2DEG in a direction determined by the direction of the magnetic field. This results in a net transport of electrons along the circumference of the 2DEG, i.e. a persistent current. Fig. 5.7 shows a (circular) section of 2DEG in an energy-position landscape. The (two) Landau levels result in just as many edge states at the Fermi energy and each edge state will contribute to the circulating current.
At a magnetic field B electrons travelling along the edge through a local electrostatic field E have a velocity of approximately $v \cong E/B$, and so *each electron* in an edge state contributes a current

$$i = ev/L \cong eE/LB \qquad (5.8)$$

with L being the length of the circumference of the 2DEG section. The current due to the circulating electron generates a magnetic moment $M=iS$, where S is the area of the 2DEG involved.

Problem: Estimate the magnetic moment for the case of a single edge state, taking $S=1$ μm^2 and a typical value of $E \sim 10^4$ V/m for the electric field at the edge. (Note: to estimate the number of electrons involved assume a linear gradient of the electrostatic potential at the edge). Compare the calculated M with the external field required to establish the IQH state with one edge state.

After these two examples based on preceding discussions in the next sections we will introduce persistent currents in normal conducting rings. In the first subsection, 5.3.a, we start with the basic theory underlying the phenomenon, starting from a ballistic 1-dimensional ring to see the role of quantum eigenstates. This is generalised by introducing scatterers (and thus going from ballistic to the diffusive case) and allowing multiple mode occupation. Also the mechanism of period halving in multi-ring structures will be introduced. Next, in subsection 5.3.b. the presently available experimental results are discussed. We finalise the chapter by briefly discussing the relation of the persistent current problem and the AB effect.

5.3.a. *Theory of persistent currents in rings of normal conductors*

In this subsection we introduce the main aspects of the theory of persistent currents. It will be shown that persistent currents arise because of the existence of well defined quantum eigenstates in the ring. An electron occupying such an eigenstate has a non-zero velocity, which results in a stationary circulating current. Most notably, this current is an *equilibrium property* of the electron in the ring. The magnitude of the persistent current depends on the E-k and/or E-B relation, with B and applied magnetic field that pierces through the opening of the ring. We will see how elastic scatterers in the ring affect the E-k spectrum, and in this way the size of the circulating current.

Figure 5.8 shows a metallic ring with a circumference of length $L=2\pi R$, placed in a magnetic field B such that a flux Φ is enclosed by the ring. The width of the ring is taken to be such as to accommodate just one single mode or subband, i.e. roughly speaking it is approximately half a Fermi wavelength. In this way the system is 1-dimension (1D). We

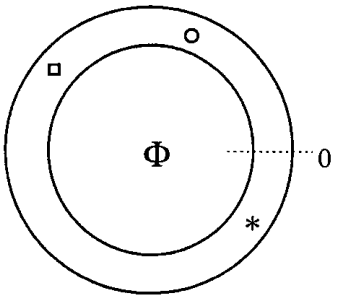

Figure 5.8. Narrow isolated metallic ring with elastic scatters.

assumed that electrons travelling around the ring preserve their phase during at least one round-trip, i.e. $L<l_\phi$. The ring may contain a few elastic scatterers, which we initially assume to be weak. Electrons travelling around the ring will experience the same conditions again (e.g. the potentials due to the local scatterers) each time they have completed one round-trip. Stated differently, they will behave as if they are travelling in a *periodic potential*, with a period of length L. Fig 5.9 shows this periodicity more explicitly by "unfolding" the ring into a strip with segments of length L each.

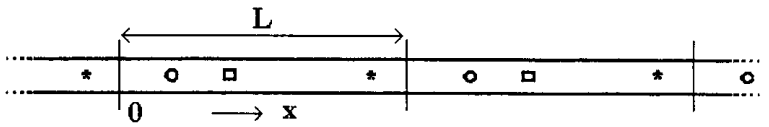

Figure 5.9. The periodic system resulting from cutting, unfolding and repeating the ring structure of Fig. 5.8.

The system we thus obtain is completely identical to the periodic structure experienced by an electron in a solid state crystal lattice. This allows us to use the same techniques to evaluate its properties. From quantum mechanics we know that this periodic motion leads to the formation of eigenstates, with associated eigenvalues for the energy, wavevector and velocity. To simplify the discussion at this stage, we assume that the scatterers are absent; we will re-introduce them later again. At zero magnetic field we immediately can deduce the eigenvalues for the k-vectors:

$$k_p = \pm p\frac{2\pi}{L} \qquad (p=0, 1, 2,...) \qquad (5.9)$$

The quantum number p labels the states. As discussed before in section 5.2, applying a magnetic field will affect the phase of the electron via the vectorpotential (eq. 5.1), resulting in an additional phase shift $\Delta\phi$ depending on the flux Φ enclosed by the ring (eqs. 5.2 and 5.3)

$$\Delta\phi = 2\pi\,\Phi/\Phi_0 \qquad (5.10)$$

with Φ_0 denoting the flux quantum for single electrons, $\Phi_0 = h/e$. Evidently this phase shift will affect the eigenvectors k_p, resulting in a modified condition for establishing a bound state

$$k_p(\Phi)L - \Delta\phi = p2\pi \tag{5.11a}$$

or

$$k_p(\Phi) = (p + \frac{\Phi}{\Phi_0})\frac{2\pi}{L} \tag{5.11b}$$

From this condition for the quantisation of the momentum we immediately can derive the velocity and the (kinetic) energy of the states of quantum number p

$$v_p(\Phi) = \frac{\hbar}{m}k_p(\Phi) = \frac{\hbar}{m}(p + \frac{\Phi}{\Phi_0}) \tag{5.12}$$

$$E_p(\Phi) = \frac{\hbar^2}{2m}k_p^2 = \frac{\hbar^2}{2m}\frac{4\pi^2}{L^2}(p + \frac{\Phi}{\Phi_0})^2 \tag{5.13}$$

Fig. 5.10 shows the resulting E-Φ-diagram, with the quantum number p labelling the successive parabolas. Note the similarity to the E-k diagram as obtained in the common solid state case. As anticipated the figure shows periodicity in the number of flux quanta contained within the area of the ring.
The current carried by the circulating electron can be calculated simply by

$$i_p = \frac{dQ}{dt} = \frac{-e}{L/v_p} = -\frac{ev_p}{L} \tag{5.14}$$

The current carried by such a bound state can also be obtained in a more general way. To

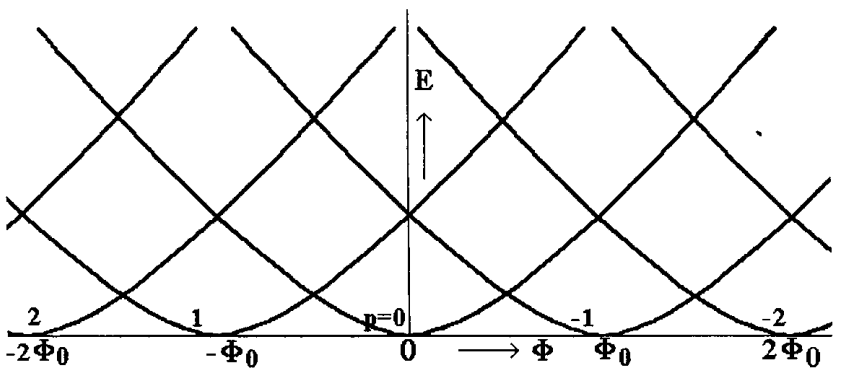

Figure 5.10. The E-Φ -diagram for electron states in the 1D ring of Fig. 5.8

see this we calculate the derivative of the kinetic energy to the flux Φ

$$\frac{dE_p}{d\Phi} = \frac{\hbar^2}{m} k_p \frac{2\pi}{L\Phi_0} = \frac{h}{L\Phi_0} v_p = \frac{e}{L} v_p(\Phi) \qquad (5.15)$$

Noting that the two right-hand side expressions of eqs. (5.14) and (5.15) are equal, we conclude that the current can be written as

$$i_p = -\frac{dE_p}{d\Phi} \qquad (5.16)$$

This equation is the well known thermodynamic relation between the magnetic moment M ($=iS$) and the derivative of the (Gibbs free) energy to the magnetic field B ($= \Phi/S$), with S denoting the area enclosed by the circulating current i which generates the magnetic moment M. Note that i_p is the current contributed by a *single electron in a specific state labelled by p*. As commonly the magnetic field employed in these experiments is small, the spin degeneracy will not be lifted and so eq. (5.16) has to be multiplied by the factor g_s=2 to obtain the total current per fully occupied level (i.e., two electrons, one spin up and one spin down).

Before continuing to show how one obtains the total current resulting from the contributions of all the electrons in the ring we first want to discuss the effect of the elastic scatterers as shown in Fig. 5.8. The effect of each scatterer that it introduces a non-zero localised electrostatic potential in the system. Given the ring shape, this leads to a *periodic potential* for the electrons as shown in the unfolded system of fig. 5.9. From introductory solid state physics we know that the non-zero value of the periodic potential results in Bragg reflection of the electron waves and *the formation of energy gaps and bands*. This is shown in fig. 5.11. Because of the formation of energy bands a new set of quantum numbers n is introduced, which enumerates the bands starting from the one that

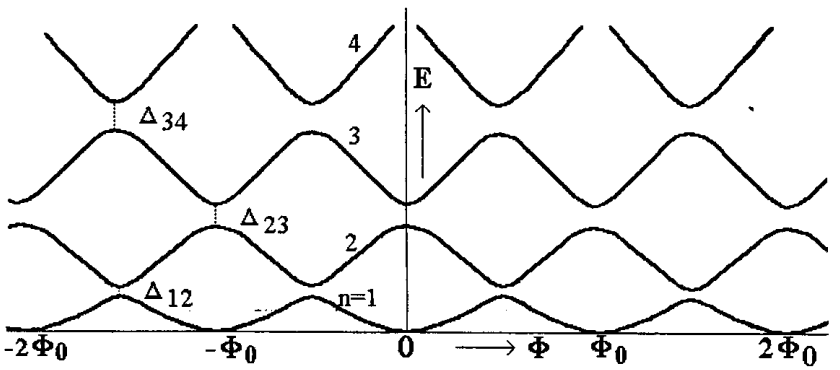

Figure 5.11. The finite potentials of the elastic scatterers in the ring of Fig. 5.8 lead to the formation of gaps in the parabolic E-Φ -diagrams of Fig. 5.10.

is lowest in energy. The size of the gaps can be derived in a simple way from the potential $V(x)$ along the ring (x represents the position coordinate running along the ring). As $V(x)=V(x+L)$ is periodic, it can be rewritten as a Fouriersum by (see e.g. Kittel, Introduction to Solid State Physics)

$$V(x) = \sum_{k_p} U_k \exp(ik_p x) \tag{5.17}$$

This allows one to calculate the size of the gaps as

$$\Delta_{12} = 2\,U_1,\ \Delta_{23} = 2\,U_2, \ldots. \tag{5.18}$$

So, strong potential variations $V(x)$ generally will lead to an increase in the gaps with a simultaneous reduction of the width of the bands. Stated differently, an increase in disorder (or: a reduction of the elastic mean free path) leads to larger gaps and narrower bands. Equivalently, crossing from the nearly free electron case with its weak scattering to the tight binding regime with strong scattering leads to an increase in the localisation of the electrons, and we anticipate that this will be accompanied by a reduction of the average velocity of the electrons in the states, i.e. the current. We return to this below.

Now all the ingredients to calculate the *total* current in the ring are available, by appropriately summing all individual currents in each band. For the case of the parabola of the clean (impurity free) case, each state contains two electrons at maximum, due to spin. Equivalently, for the case of elastic scattering, each band only can accommodate two electrons. So, we assume 2N electrons in the ring occupying N bands (n=1,2,3,..,N). Referring to fig. 5.11 it is obvious that the maximum current (or, the maximum slope of E versus Φ, see eq. (5.16)) occurs at $\Phi \cong \Phi_0/4$. For the case of small gaps, i.e. for weak disorder, the *typical maximum* current in band n for this value of Φ can be obtained from eqs. (5.11b, (5.13) and (5.16) as

$$i_n \approx (-1)^n g_s \frac{eh}{m}\frac{1}{L^2}((n-1)+1/4) \tag{5.19}$$

The prefactor $(-1)^n$, indicating the sign of the derivative of E with respect to Φ, alternates for successive bands with quantum numbers n, a property which is immediately evident from figure 5.11. Consequently, *currents of successive bands largely cancel, yielding a sum that is approximately equal to the contribution of a single band*, say the topmost band with label N. Thus as an order of magnitude estimate for the total current of N filled bands at $\Phi \cong \Phi_0/4$ we find

$$|I_N| = |\sum_{n=1}^{N} i_n| \sim |i_N| \approx g_s \frac{eh}{m}\frac{1}{L^2} N \approx 2e\frac{v_N}{L} \tag{5.20}$$

Problem: derive the last "equality" of eq. (5.20)

The argument for the *current cancellation of successive bands* is independent of the scattering strength. So, the "equality" $|I_N| \sim |i_N|$ provides a way to evaluate the *total current* for any scattering strength, assuming the bandstructure is known (which is by no

means obvious!) so that the current in the N-th band, $|i_N|$, can be evaluated using eq. (5.16).
From eq. (5.16) one also can understand how the current will be affected by an increase in the disorder in the ring. Stronger scattering will lead to larger bandgaps (eq. (5.18)) and consequently to narrower bands. These narrower bands have a smaller slope of energy with respect to the flux, resulting in a reduction of the current per band (eq. (5.16)). From the first part of eq. (5.20) it is then obvious that the total current will be reduced compared to the nearly-free electron case of small scattering.

Problem: Calculate the total current for a metallic ring of L=1 μm in the weak scattering regime. How many electrons and bands are involved? (Answ: ~ 1 μA)

To obtain a rough estimate of the persistent current in the case of increased scattering we do not need to evaluate the bandstructure of a disordered ring. Effectively an increase of the scattering makes the electron transport diffusive by the time the elastic scattering length l_e becomes considerably smaller than the length of the circumference of the ring, L. For a strip of size L carrying N_{ch} modes we found for the conductivity within the Drude model (see eq. (2.5))

$$\sigma_{Drude} = g_s \frac{e^2}{h} N_{ch} \frac{l_e}{L} \qquad (5.21)$$

i.e., it is reduced by a factor l_e/L as compared to the ballistic case. Note that the reduction of the conduction has an elastic, non-dissipative origin and will not affect the phase *coherence* in the system! The same factor l_e/L can be introduced in eq. (5.19) to obtain an *order of magnitude* estimate for the persistent current in the diffusive regime, yielding

$$i_n \approx (-1)^n \frac{l_e}{L} \frac{eh}{m} \frac{1}{L^2} ((n-1)+1/4) \qquad (5.22)$$

A word of caution is appropriate here. Including the effect of elastic scattering by the introduction of the prefactor l_e/L should be taken as a crude first order guess. In particular for the case of few channels (so including the 1D case we have been discussing here) its validity is rather limited!

Now that we have discussed the effect of elastic scattering in some detail, the question arises on the effect of inelastic processes on the magnitude of the persistent currents. This problem can be approached largely along the same lines as in the preceding section 5.2 on the AB effect. Inelastic scattering will reduce the phase coherence length l_ϕ and time τ_ϕ, and consequently will decrease the lifetime of the eigenstates of the ring. As usual this leads to a broadening of the energy levels of these states. By the time the broadening of the levels becomes comparable to the typical distance between the bands the bandstructure will become disrupted and the current will become suppressed significantly. This suppression will be given by the same factor as before (eq. (5.6a))

$$i_n = i_{n0} \exp(-\frac{L}{l_\phi}) \qquad (5.23)$$

Before continuing the discussion of the theory of persistent currents we first take a small sidestep to some experimental details. This is in order to estimate the magnitude of the total current in a ring, and how it has to be measured.
Experimentally, in the case of a ring fabricated by metal evaporation, the typical thickness of the metallic sheet will be some 30-100 nm (see also Appendix A), containing typically 10^6-10^8 electrons. Assuming diffusive scattering at the substrate-metal interface, l_e will be of the same order of magnitude. Consequently in a ring of $L\sim$ 1 μm the persistent current will be reduced by a factor $l_e/L\sim$10-30 compared to the ballistic case (see eq. (5.22). As we have found the typical current for the ballistic case to be <~1 μA, we end up with $|I_N|<\sim$0.1 μA in the diffusive regime: a rather small current! This current not only is rather small, but in addition it can *not* be measured in the conventional way by "cutting" the ring and including a current meter in the circuit. The inclusion of such meter (based on classical, dissipative phase breaking mechanisms!) will disrupt the quantum eigenstates of the ring and thus suppress any persistent currents associated with them. The only method to determine these currents is by measuring the magnetic moment $M=iS$ resulting from the circulating currents, e.g. by employing a magnetometer like a SQUID. We will return to it later in the chapter when we discuss the experimental results (see also Appendix B). The matter of experimental accessibility is brought up here to pose the obvious question: is there a way to increase the total magnetic moment resulting from persistent currents? Two possibilities may come to one's mind: employing a ring accommodating more than one channel; or using a number of separate identical rings.

Let us first consider the problem of a single ring containing more than one channel, say M channels (or modes/subbands) enumerated by m=1, 2, 3, ... In the case of a complete absence of elastic scattering the M channels will behave independently, with each channel forming a set of bands. Assume mode m to contain N_m filled bands, i.e. $E_{N_m} = E_F$ and $E_{N_m+1} > E_F$. Due to the complete independence of the modes a multichannel equivalent of the bandscheme of Fig. 5.10 is results, and each subband will show up as a set of parabolas, of course again periodic in Φ_0. However, each set will have its bottom at an (increasingly larger) subband minimum E_{m0}, which is as usual determined by the associated quantised perpendicular wavevector k_m (see chapter 2). For each subband m, containing N_m filled bands, the current per state can be calculated from eq. (5.16), while the total net current *per subband* is obtained from eq. (5.20). To calculate the total current we have to sum the contributions of all individual subbands. In doing so we again have to consider the argument of partial cancellation, this time resulting from the prefactor $(-1)^{N_m}$, which will be (rather randomly) positive or negative for each individual channel with N_m filled bands. As a consequence the resulting sum again will be similar to that given by eq. (5.20), i.c. of the order ev_{max}/L, with v_{max} denoting the velocity of the highest lying occupied state of the lowest subband, or stated differently, from the state with the largest kinetic energy or velocity.
So, in conclusion, increasing the width of the ring to accommodate more than one channel, does *not* increase the net typical persistent current in the ring, despite the increase of the number of electrons in the system!

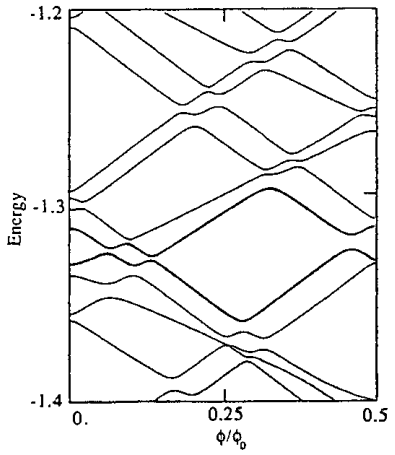

Figure 5.12. Part of the energy-flux bandstructure for a disordered ring in the weak scattering limit; it contains M=10 lateral subbands.

Using approximative methods it is possible to calculate the bandstructure of disordered systems of the nature we have been discussing. Although we will not go into any detail of such calculation, an example of the complexity of such bandstructure of a multichannel ring is shown in figure 5.12 (H. Bouchiat et.al, J. Phys. France 50, 2695 (1989)). Here the limit of weak scattering is taken. The ring contains M=10 subbands.
Only the flux range 0-$\Phi_0/2$ is shown, as the current will be symmetric around Φ_0=0 and periodic in one flux quantum Φ_0. In the diagram the opening of (small) gaps due to the weak disorder is clearly visible. Note that none of the states ever *crosses* another state: the gaps effectively make all states to avoid each other! This very general behaviour of eigenstates in complex systems is called *level repulsion*, something we will come back to in Chapter 9. Note also that no longer the maximum slope (and so the maximum current) occurs at $\Phi_0/4$: this is a direct consequence of the mixing of the individual subbands by the elastic scattering.

Now we want to address the second possibility raised with respect to increasing the total magnetic moment due to persistent currents, i.e. by combining a number of (nominally) identical rings. Here we will again encounter the effect of *period halving*, i.e. the magnetic moment due to the total circulating current shows a periodicity $\Phi_0/2$, similar to what was found in the AB/AAS effect in a multi-ring configuration in the preceding section 5.2 (see fig. 5.5).
Metallic rings of micrometer diameter typically contain at least 10^6 electrons. If an ensemble of nominally identical rings is fabricated the number of electrons residing in one particular ring, however, may differ considerably. Depending on the quality of the fabrication process, variations up to ~ 1% are realistic, which is equivalent to at least 10^4 electrons. In addition the details of the bandstructure of each ring will differ as the actual positions of the scatterers in each individual ring will be different. Noting that the difference of *one single electron* may already *reverse* the direction of the current (see eq. (5.19)), it is clear that these much larger variations will have a profound effect. So, nominally identical rings will differ widely when it comes to thermodynamic equilibrium

electronic properties. Let us look to the consequences for the magnetisation of an ensemble of rings in a little more detail.
In order to keep the discussion relatively simple we assume an ensemble of three 1D rings in the weak scattering regime, each of size L. Each of the R=3 rings, indicated by r=1, 2 and 3, contains a different number of electrons N_r and again for simplicity we assume the

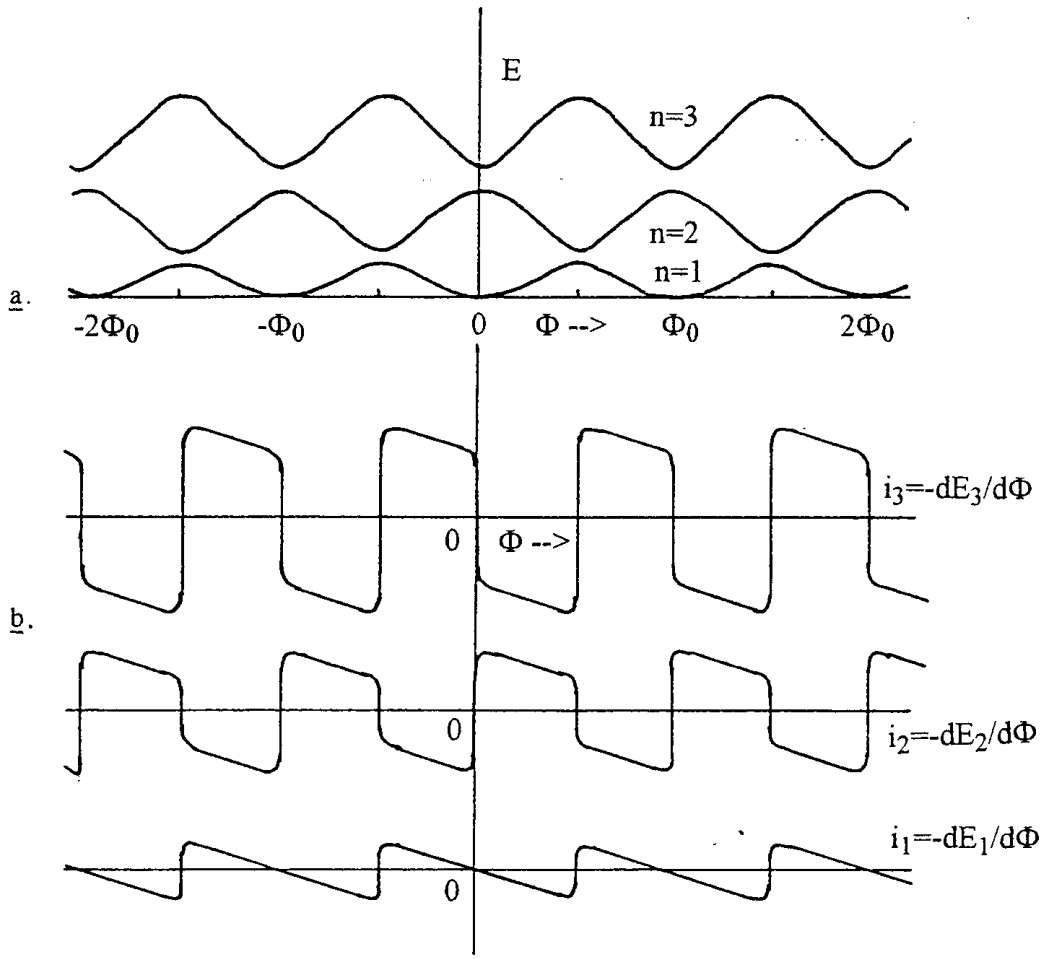

Figure 5.13. Persistent currents in an ensemble of 3 rings, containing 1, 2 and 3 electrons respectively; a. the energy diagram showing 3 bands: for the ring containing 3 electrons all bands are occupied, bands 1 and 2 will be filled for the ring with 2 electrons, while only the lowest band is filled for the ring containing a single electron; b. the derivative of energy versus flux for each of the bands, providing the persistent current per (filled) band.

first ring to contain N_1=1 electron, the second N_2=2 and the third N_3=3; we do not take the spin into account, so g_s=1. Fig. 5.13a shows the resulting bandstructure E-Φ, drawn for ring r=3, with the three bands involved. Note that the *details* of the bandstructure of the rings 1 and 2 will be different (e.g. the gaps may differ in size), but *globally* they will behave similarly. For ring 1 (containing just one electron) only the lowest band is filled, while for the second ring bands 1 and 2 are occupied. In Fig 5.13b the currents $i_{3,n}(=-dE_{3,n}/d\Phi)$ for ring 3 are shown, for each individual band n=1, 2 and 3. Note again that the currents for ring 1 and 2 may differ in magnitude because of the difference in e.g. the size of the gaps, but the *global* shape of $i_{1,n}$ (n=1) and $i_{2,n}$ (n=1,2) will be rather similar.

The next step is to calculate the total current per ring as $I_r = \sum_n i_{r,n}$ for the 3 rings r=1,2 and 3 (=R). This is shown in figure 5.14. This figure also shows the mean value $\langle I_R \rangle = (I_1+I_2+I_3)/R$ of the 3 rings. From the figure it is clearly seen that the mean current shows a pronounced *halving of the period, i.e. a* $\Phi_0/2$ periodicity. This is a characteristic feature resulting from the averaging process; it becomes increasingly pronounced if

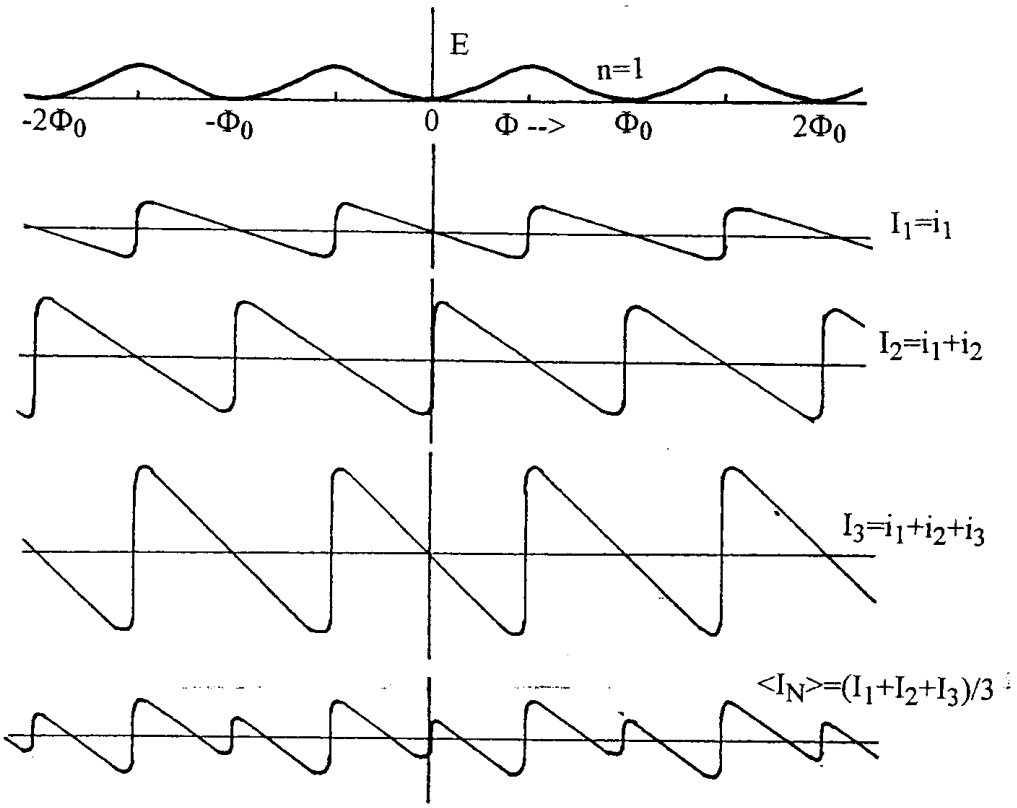

Figure 5.14. The calculated total persistent current for each ring, I_1, I_2 and I_3, and the resulting mean value of the currents in the three rings, $\langle I_3 \rangle$.

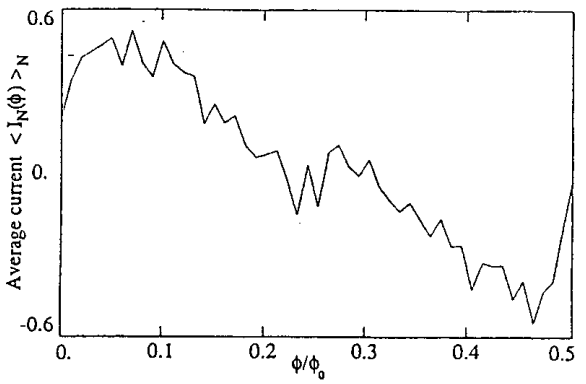

Figure 5.15. Mean persistent current for a large ensemble of similar rings. The number of filled bands for each ring, N_r, is distributed evenly between 150 and 250.

the averaging is performed over larger ensembles of rings (or larger R). Note also that the magnitude of the mean current is comparable to that of the current of a single ring.
Now we are ready to evaluate the total magnetic moment due to the circulating persistent currents in all three rings. If S is the area per ring, this moment is given by
$M= M_1+M_2+M_3= S(I_1+I_2+I_3)= S*R*<I_R>$.
This result leads to two important conclusions. First, *the total magnetic moment scales linearly with the number of rings*, which means that it is experimentally useful to employ a set of rings. Second, the total signal for the set of nominally equal rings *shows period halving*, contrary to the case of a single ring where the persistent current shows oscillations periodic in a full flux quantum.
Figure 5.15 shows the results of a calculation for a set of rings in the limit of weak disorder; the number of filled bands per individual ring ranges between 150 and 250 [H.Bouchiat et.al.]. Clearly in this much more realistic case the characteristic period halving which we have found in the simple example is evident, stressing the universality of this phenomenon.
The suppression of the *h/e* component in the persistent current (or magnetic moment) while preserving the *h/2e* component in averaging over a number of independent rings, basically has the same origin as the survival of the AAS component for the case of the multi-ring AB/AAS conductance as discussed around figure 5.5. It originates because the phase of the half flux quantum component always has a specific behaviour around zero flux. This symmetry forces the individual contributions to sum "coherently", while the one flux quantum contributions add randomly.

Problem: discuss the case that the sizes of the rings contained in the set differ: consider in particular the effects on the amplitude in dependence of the applied flux.

5.3.b. *Experimental results of persistent currents in single and multiple rings*

In this subsection we will consider three cases: a single metallic ring in the diffusive regime, a single semiconductor ring in the (quasi-)ballistic regime, and an experiment on a set of approximately 10^7 metallic rings. It should be noted that this sequence is historically incorrect, as the experiment on the set of rings preceded the single metal and semiconductor ring cases, basically due to the large experimental difficulties for the single ring case.

1. Single metallic ring in the diffusive limit.

In 1991 Chandrasekhar et.al. (Phys Rev. Lett. 67, 3578 (1991)) presented their experimental results obtained on a single gold ring. The ring had a diameter of 2.4 μm, a width of 90 nm and a thickness of 60 nm (Fig 5.16b). A rough estimate based on the width and thickness indicates that some $M=10^5$ transverse modes are occupied in this device. From resistance measurements on a simultaneously evaporated gold strip the elastic mean free path is found to be ~70 nm and from weak localisation measurements (see chapter 2, section 3) on a simultaneously evaporated strip a phase coherence length l_ϕ~ 10 μm (at T=50 mK) is obtained, the last one depending particularly on the density of magnetic impurities in the gold. Fig 5.16a shows a (strongly simplified!) diagram of the set-up for the measurement.

It consists of a SQUID magnetometer, two coils of superconducting wire to pick up the magnetic moment (one of which contains the ring), and two field coils to generate the magnetic flux through the ring (see also Appendix B). The coils are configured to form a so called (first order) magnetic gradiometer, allowing the discrimination between magnetic signals from the ring relative to those from the environment. Any magnetic signal induced in the two pick-up coils *simultaneously* is suppressed as these are *counter wound*, while the signal due to the magnetic moment of the ring induced in a single coil is transferred to the SQUID detector.

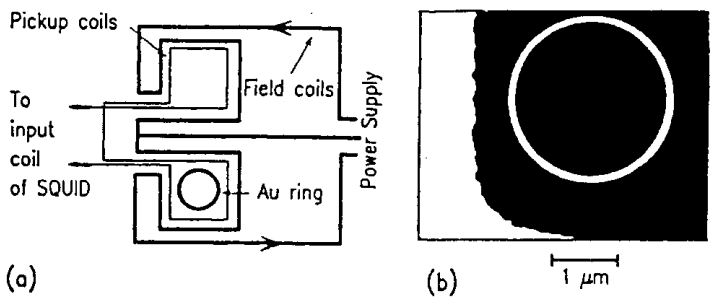

Figure 5.16. a. Experimental configuration to measure the magnetic moment resulting from persistent currents. The field coils generate the flux; the pickup coils sense the magnetic field resulting from the applied flux and the contribution from the magnetic moment of the ring. This total signal is fed to a SQUID magnetic detector. As the pickup coils are counter wound, they form a (first order) gradiometer, leaving the (unbalanced) signal from the ring while suppressing the (balanced) signal from the applied flux. b. An SEM image of the single Au ring of ~ 2.4 μm.

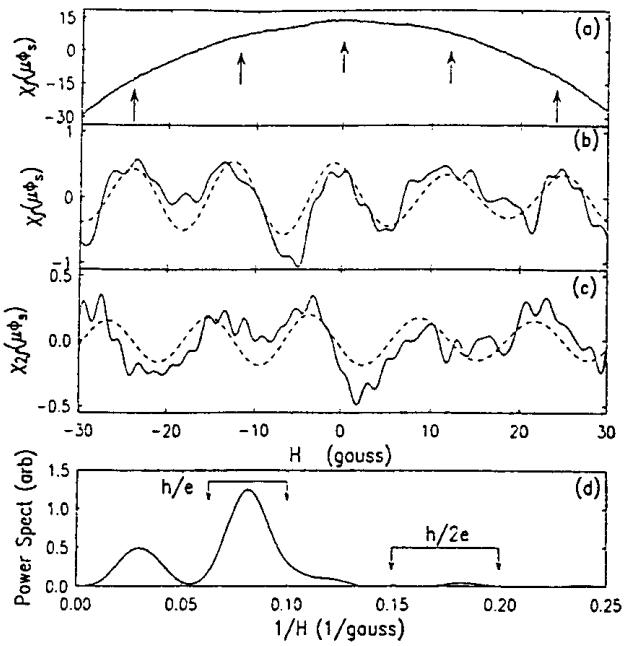

Figure 5.17. The first (a, b) and second order (c) derivatives of the magnetic moment of the Au ring. a shows the raw data directly derived from the SQUID detector. Subtracting a (fitted) second order polynomial results in b and c (solid lines). d shows the Fourier transform of the data of b, with a clear peak at a period of single flux quantum.

To enhance the sensitivity the measurement is performed by adding an AC modulation to the flux applied by the field coils, i.e. $\Phi = \Phi_{DC} + \Phi_{AC} = S*B_{DC} + S*B_{AC}*\sin(2\pi*fmod*t)$, with $S*B_{DC} \sim \Phi_0/10$ typically. The signal induced in the SQUID can be synchronously detected in a lock-in detector, not only at the modulation frequency *fmod*, but also at its harmonics $n*fmod$ (n=2,3,4,..). Detecting at the n-th harmonic effectively means a measurement of the n-th order derivative of the total SQUID signal with respect to the applied flux $S*B_{AC}*\sin(2\pi*fmod*t)$. For more details one should consult Appendix B.

Fig 5.17 shows the results obtained by detecting at *fmod* and *2fmod*, in dependence of the applied DC magnetic field B_{DC} given in Gauss (B=1 T=10^4 Gauss). Fig 5.17a shows the total signal obtained at the modulation frequency. It shows a parabolic behaviour superimposed with weak oscillations. Subtracting a (least square fit) second order polynomial results in Fig 5.17b, displaying the oscillation more clearly. Note that, despite extensive signal averaging (a number of independent measurements were combined to obtain this trace) to enhance the oscillatory signal, the ratio of signal-to-noise is only ~5:1! This stresses the difficulties encountered in this type of experiments. Fig 5.17c shows the signal obtained at the second harmonic *2fmod*. To demonstrate the occurrence of the oscillatory component in the signal shown in Fig. 5.17b its Fourier spectrum is displayed in Fig. 5.17d. A clear peak at a "frequency" $1/\Delta B$=800 T^{-1} is evident. Taking into account the area of the ring this corresponds to a single flux quantum *h/e* being added to the ring per oscillation. This is in full agreement with the theory discussed before.

Problem: check the statement on the period using the given diameter of the ring.

In contrast to the good agreement of the period a serious problem arises if the amplitude is considered. Without going in all the details of the experiment one finds that the amplitude of the measured signal is approximately 30-50 times *too large* as compared to the estimate based on eq. (5.22). We will return to this point briefly at the end of this section.

2. Single semiconductor ring in the quasi-ballistic regime

The ring is realised in a 2DEG in a GaAs/AlGaAs heterostructure, obtained by dry ion beam etching (D. Mailly et.al., Phys. Rev. Lett. 70, 2020 (1993)). The bulk 2DEG has a mobility of ~100m^2/Vs and an electron density of ~3.5*10^{15} m^{-2}, yielding a Fermi velocity v_F~2.5*10^5 m/s and an elastic mean free path l_e~ 10 μm (see chapter 1). With an effective width of ~160 nm (taking into account the depletion resulting from the etched

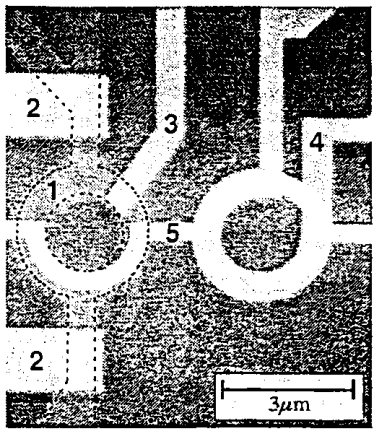

Figure 5.18. Sample layout of the ring used to measure the persistent current in a 2DEG semiconductor. (1) denotes the etched ring with gates (2) (to allow AB measurements) and (3) (to allow suppression of the persistent current. (5) is (a part of) the SQUID

walls) approximately M=8 modes will be occupied in the ring. Apart from some details the experimental approach strongly resembles the preceding one, again employing a SQUID gradiometer to detect the magnetic moment of the ring. Fig 5.18 shows the sample configuration, with only the first part of the SQUID put into place. Note the additional gate structures (2) and (3) in the sample. The first gate pair allows the

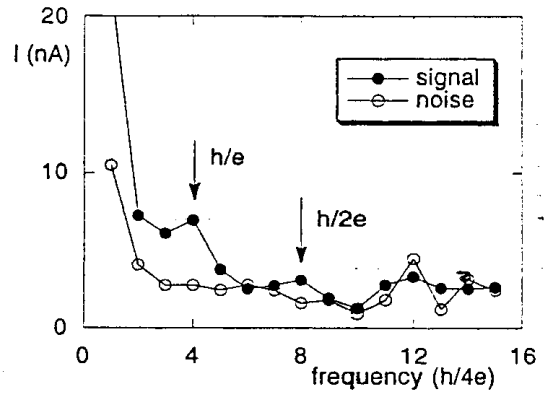

Figure 5.19. Measured persistent current in the 2DEG ring of Fig. 5.18. The figure shows the Fourier tranform of the magnetic moment detected by the SQUID, expressed in terms of an equivalent current.

connection of the ring to external leads to perform AB measurements to be done. Gate (3) controls the current flow in the ring: with a negative voltage applied to it the persistent current can be suppressed, allowing the measurement of the magnetic moment with and without the persistent current flowing. Figure 5.19 shows the results obtained.
Two rather weak peaks can be seen in the Fourier spectrum, with the *h/e* peak being most pronounced. It is of considerable interest to note that in this case, where the electrons in the ring behave approximately ballistically, the measured amplitude of the persistent current of ~5 nA is in *good agreement* with the theoretical prediction based on eq. (5.20) or (5.22). We will discuss this further after presenting our last experiment.

Problem: check this statement on the value of the current.

3. Multiple metallic rings in the diffusive limit.
The third experiment, -which is historically the first of the three we discuss here-, concerns a set 10 million (nominally) equal copper rings and is due to L.P. Levy et.al. (Phys. Rev. Lett. 64, 2074 (1990)). Also in this case the set-up largely resembles the one discussed around figure 5.16a. The result obtained by detecting at the third harmonic $3*f_{mod}$ is presented in Fig. 5.20. Although only a limited number of data points is

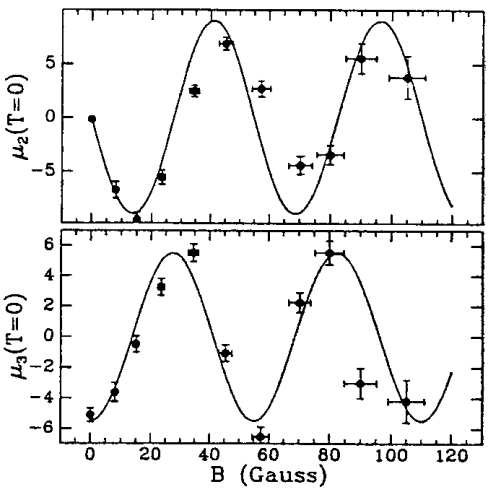

Figure 5.20. Measured magnetic moment of an ensemble of 10^7 copper rings, showing persistent currents. Both the signal at 2f and 3f is shown. As ΔB=130 Gs corresponds to 1 flux quantum through a ring, period halving is evident.

available a clear oscillation is visible. Noting that a single flux quantum through a ring corresponds to 130 Gauss, it is clear that the oscillation shows a period of *half a fluxquantum*, which is nicely in accordance with the prediction given for the multiple-ring case. Concerning the amplitude the evaluation of the magnitude of the magnetisation again leads to a size that is considerably larger than predicted via eq. (5.22), in this case by a factor of approximately 30!

From the three experiments discussed we conclude that good agreement with theory exists on the periodicity of the magnetic moment, with Φ_0 for a single ring and $\Phi_0/2$ for the case of an ensemble of rings. A much less favourable picture arises for the amplitude of the persistent currents. For the ballistic, weak elastic scattering case with only a small number of modes in the ring encountered in the second example of the high-mobility

2DEG, where $l_e/L \sim 1$ or even larger, agreement with theory is good. However for metallic rings, with the electrons moving diffusively, the measured amplitudes are much too large, the discrepancy being at least as large as one order of magnitude! This serious problem is not solved at the moment this text is updated (mid 1997). Various additional mechanisms have been introduced, mostly based on the regulating influence of electron-electron interaction, but none has been completely successful up to now.

5.4. Final remarks

In the preceding two sections 5.2 and 5.3 we have introduced two phenomena that originate from the interference of electron waves in ring-shaped solid state structures. Both these phenomena show a periodic behaviour, with a fundamental period given by the change of the flux that penetrates through the area enclosed by the ring by one flux quantum $\Phi_0=h/e$. In both cases phase coherence is a crucial requirement for the effect to arise, as otherwise interference effects are suppressed.
In discussing the AB and AAS effects in section 5.2 we described the effect as the coherent transmission (and reflection) of electron waves through the ring, allowing such wave to split at one lead-ring junction and reunite at the other. By taking into account the phase shift induced by the magnetic field (via the vector potential) a periodic modulation of the total transmission probability is found, leading to an oscillatory dependence versus the applied flux of the conductance.
In evaluating the persistent currents in section 5.3 we took a different view. Here we assumed the ring to form eigenstates, the energies of which were shown to be flux dependent, again via the vector potential affecting the k-vector and in this way the phase acquired during one roundtrip. The equilibrium state current transported in a state derives from the flux dependence of the energy of that particular state.
Basically, also the AB and AAS effect could have been introduced by starting from the eigenstate picture. In this picture the system is represented by having the states in the leads couple to the eigenstates of the ring. Pictorially this implies that one has to evaluate the transmission coefficient for a certain state in the left lead to a certain state in the right lead via one eigenstate of the ring. After summing over all (occupied) states in the input and output leads one finds the total transmission in going from left to right, i.e. the total conductance. Evidently, while the eigenstates of the ring depend on the flux through its central area, the overall coupling will depend on it, and this will again be periodic in the flux quantum. One may denote this as *resonant "tunnelling"* through the eigenstates of the ring.

General references to the subject:

1. "The Feynman Lectures on Physics", (Addison-Wesley, 1964), Vol 2, pp 12-15
2. The Aharonov-Bohm effect: Physics Today, January 1986, p 17
3. Persistent Currents: Physics Today, April 1992, p 17